Section 1
Team 5
May 7, 2019

E80 Final Report

Marco Conati, Katharine Larsen, Erika MacDonald, Yaqub Mahsud

***Abstract*-- During this project, we created an autonomous underwater vehicle (AUV) that navigated using proportional control. This AUV measured turbidity, clarity, and wind speed in order to observe how wind speed affects turbidity and clarity. We 3D printed a nephelometer and anemometer for turbidity and wind speed measurements respectively. Additionally, we used photodiodes to measure how well light permeated the surface as a metric for clarity. Tests for these sensors and navigation took place through deployments at Bernard Field Station (BFS), pools across the Claremont Consortium, and Dana Point. Notably, we found that an increase of 82% in turbidity corresponded to a 22% increase in clarity.**

I. Introduction

Turbidity and clarity are both visual properties of a body of water, with turbidity referring to the amount of particles suspended in the water and clarity referring to water visibility. Both turbidity and clarity are important measurements for oceanic health. The more sediment present in the water, the less light is able to reach oceanic plants [17]. Additionally, high sediment concentrations can carry pathogens and have potentially negative health effects on aquatic life. Furthermore, there is some documentation mentioning a correlation between wind speed and turbidity [19]. Since wind speed can differ based upon location, measurements may be taken at different locations to see the influence of wind speed on clarity and turbidity. As a result, we wanted to create an autonomous underwater vehicle (AUV) that could use GPS locations and proportional control to navigate and measure wind speed, turbidity, and clarity both above and below the water's surface to try to reaffirm this correlation, and measure trends in these properties over long periods of time.

This paper will begin by explaining our scientific and engineering goals for the project, then it will describe the sensor selection process, followed by a circuit and robot design section, then an explanation of the expected modeling. Then, getting into the heart of the project, we will describe the experimental procedure for the project, and explain the results that were obtained from various deployments. Finally, we will compare our experimentally obtained results to our predicted results, and provide a conclusion that gives a brief review of the project and touches on what we did well and areas that could be improved in the future.

II. Scientific and Engineering Goals

Due to the negative effects that high sediment concentrations can have on on oceanic health and aquatic life, the scientific goal of this project was to measure wind speed, turbidity, and clarity, and determine if there is a correlation present between the different measurements as the literature suggests. Wind speed should affect turbidity in two different ways. The first way in which wind speed and turbidity could be related is that increased wind speed could blow dirt, sand, and other particles into the water from the surrounding land thus causing more sediment to be present in the water and increasing the turbidity. Alternatively, increased wind speed could affect wave height and current speed which could in turn disturb sediment from the ocean floor and thus increase turbidity. Due to the added complexity of wind speed affecting current and turbidity closer to the ocean floor, and the fact that the literature showed that there is a correlation between wind speed and turbidity closer to the ocean floor, we chose to focus on how wind speed could affect surface turbidity to see if the same correlation is present.

In terms of engineering goals, we hoped to create an AUV capable of properly using GPS locations and proportional control to navigate between predetermined waypoints and collect wind speed, turbidity, and clarity data. By taking these measurements, we hoped to show that these variables are related, and come up with some quantifiable basis for their relationship. Additionally, we hoped that by creating a fully autonomous AUV we could ideally take measurements over a longer period of time to identify trends in water health over the course of a season or a year. However, due to the limited deployment time we were only able to collect data from one day and demonstrate the theoretical long term implementations of our AUV.

III. Design Process

The design process was a large aspect of this project. We split the design process into three sections: sensor selection, in which the chosen sensors are described, circuit design, in which the circuitry for the sensors is explained, and mechanical design, which includes the mechanical design for the robot.

A. Sensor Selection

In order to achieve the stated goal, we used photodiodes for both clarity and turbidity measurements and used a Hall effect sensor to measure wind speed. For turbidity measurements, we used one IR1503 IR LED [10] and two

OP950 [9] IR photodiodes and placed them in a 3D printed test fixture in order to make a nephelometer (Figure 1). The IR LED emitted light at a frequency of 480 Hz from an LM555 timer [11] in order to use synchronous detection with our IR photodiodes. One photodiode was placed directly across from our IR LED to see how much light directly passes through the water and another photodiode was placed 90 degrees from the IR LED source to measure 90 degree scattering. In order to find turbidity, we compared the values outputted from the pass through and 90 degree sensor to a calibration curve created using solutions with known turbidity values. The output of the OP950 IR photodiodes was an electrical current, so we used an MCP6004 [8] operational amplifier to create a transimpedance amplifier that would convert current to a corresponding voltage. The OP950 photodiodes were expected to output a maximum of 18 microAmps so we used a transimpedance amplifier that would convert this current to a value less than 3.3V, which is the maximum reading voltage on the Teensy.

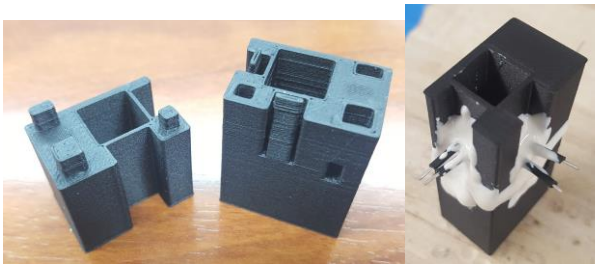

Figure 1: Photos of 3D printed test fixtures, one before epoxy and one after sensors have been epoxied.

To measure clarity, we used two visible light photodiodes (SLD-70BG2) [7]. One was placed on the portion of our robot that was floating on the surface, to get a baseline value for the the amount of light outside of the water. The second was placed underwater next to our turbidity meter to measure the amount of light that penetrated 20 cm underwater. The SLD-70BG2 outputted a maximum voltage of 0.40V, so we used an MCP6004 operational amplifier once again in order to amplify the voltage of 0.40V to a value a little less than 3.3V.

For wind speed measurements, we used a Hall effect sensor, specifically the AH9246-P-B [6]. We supplied 5V to the Hall effect sensor. We were able to supply 5V because we did not have to worry about the Teensy railing out. This is the case because the Hall effect sensor has a digital output, so we only cared about a high or low reading. The Hall effect sensor was placed in a 3D printed cup anemometer (Figure 2). A magnet was put into the base of the cup holder, and would rotate as the wind rotated the cups. The Hall effect sensor was placed in an outer radius and would output a digital output of high when there was no magnetic field and would have a digital output of low when there was a magnetic field.

Figure 2: The anemometer used on AUV

B. Circuit Design

For our turbidity sensor LED, we wanted to emit a square wave so that we could use synchronous detection on our passthrough and 90 degree photodiode sensors. To do so, we used an LM555 timer between our power supply and our LED. The circuit diagram for the LM555 is the following [11]:

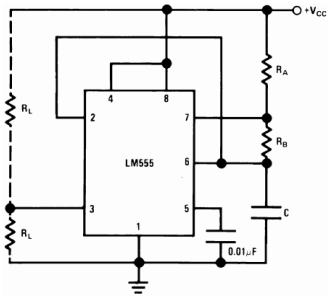

Figure 3: LM555 Circuit Diagram [11]

Where Vcc is our input 5 volts and Pin 3 is our output. We needed to set resistors Ra and Rb, along with capacitor C so that we were emitting a wave that we could detect with our Teensy. When finding the resistors, we knew that the Teensy could sample at a rate of 400 kHz so we decided to have a wave with a frequency less than 200 kHz to avoid aliasing. However, something that was not taken into account was that the Teensy program had 10 Hz sampling, so we should have kept our wave frequency below 5 Hz.

The datasheet for the LM555 lists the frequency of oscillation as:

$$f = \frac{1.44}{(Ra + 2Rb) * C}$$

Therefore, 1 kOhm resistors were used for Ra and Rb, and a 1 microFarad capacitor was used for C to have a frequency 480 Hz. However, in reality we should have used 100 kOhm resistors to obtain a frequency of 4.8 Hz to avoid aliasing.

For turbidity, we needed two photodiode circuits: one for head on detection and one for 90 degree detection. Figures 4 and 5 show the circuits for head on and 90 degree photodiodes respectively.

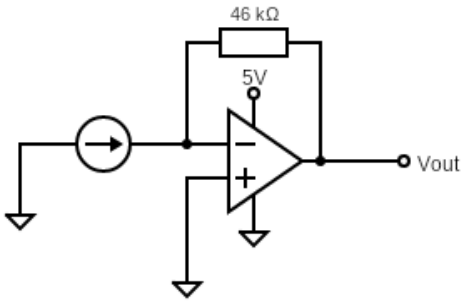

Figure 4: Circuit diagram for head on turbidity.

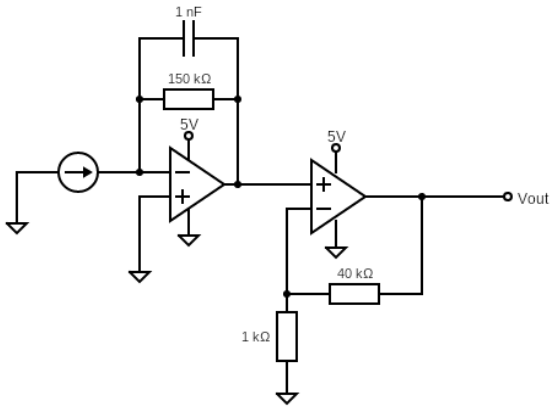

Figure 5: Circuit diagram for 90 degree turbidity.

Initially, to find the values for the transimpedance amplifier parts of each circuit, we used the fact that for a transimpedance amplifier, the equation related the current in, the voltage out, and the resistance is: $-I = V/R$. So, using that equation along with the maximum current of the photodiode and the voltage desired (a little less than 3.3V, which is the maximum for the Teensy), we were able to find general resistor values for the transimpedance circuit. We used a 46 kOhm resistor for the head-on photodiode and a 150 kOhm resistor for the 90 degree photodiode. We further amplified the output voltage from the transimpedance circuit for the 90 degree measurement. We used a non-inverting amplifier comprised of the MCP6004, a 40 kOhm resistor and 1 kOhm resistor so that there was a gain of 41. A bypass capacitor was also added to help reduce the noise in the 90 degree detection data.

Since our clarity sensors acted as voltage sources, we were able to simply use a non-inverting amplifier circuit for our clarity sensors as shown in Figure 6. To find these values, we used the fact that the gain was equal to 1 + Rf/Rg. From the datasheet, we saw that the maximum voltage that the clarity sensors could output was 0.4 V. We decided to have a gain of around six using a 5.1 kOhm resistor and a 1 kOhm resistor. By having this gain of 6.1, the maximum voltage that we would be able to obtain would be 2.4V, which would be less than the maximum Teensy analog pin voltage of 3.3 V to avoid railing out.

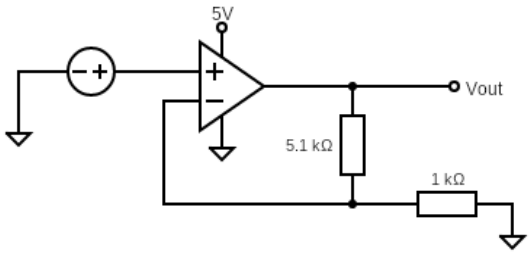

Figure 6: Circuit diagram for both clarity sensors.

As for the Hall effect sensor used for wind speed measurements, the reference circuit diagram from the datasheet was used [6]. The reference circuit diagram is shown in Figure 7.

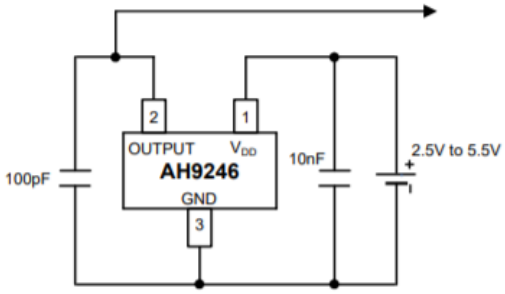

Figure 7: Hall Effect Sensor Diagram [6].

C. Mechanical Design

Given the sensors that we chose to use and the measurements we wished to take, we decided to make a surface navigating robot. As a result of this, we designed our robot to have a base that was 50 cm by 85 cm and included many different floats to ensure that the AUV stayed on the surface and had a large stable base to combat waves. In addition, four cross supports were added to create a platform for the box housing our motherboard to rest. Most of our wiring coming from the box was hidden through the PVC pipes. All of the wires are color coded in the figure below, with teal corresponding to the Hall sensor wires, blue going to the motors, red going to turbidity, and orange going to the two clarity sensors.

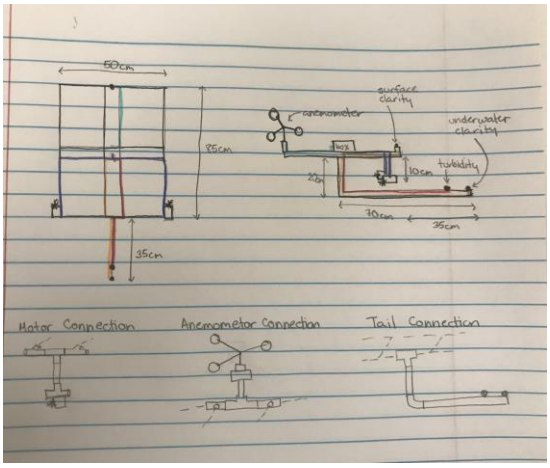

Figure 8: Mechanical Design Drawings.

The figure above also shows our sensor and motor placements. Some of our sensors needed to be underwater so we created a tail that went down 20 cm from the frame and extended out an additional 35 cm from the edge of the base. We extended the tail away from the base to prevent shadows from altering our photodiode readings. We then attached the turbidity sensor and one of the clarity photodiodes to this tail. The turbidity sensor was placed parallel to the water's surface to make it easy for water to flow through the sensor, and the clarity sensor was oriented such that it faced directly up towards the water surface. Our surface sensors, namely the anemometer and the second clarity photodiode, rested on the top platform on either side of the motherboard box. Lastly, we placed the two motors on either side of the robot away from the motherboard so that they did not affect our magnetometer readings.

In addition to the mechanical design of the robot itself we also needed to layout where the penetrator bolts would go on our waterproof box. The locations and associated connections are labeled in figure 9.

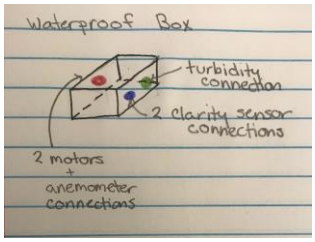

Figure 9: Penetrator Bolt Locations for Waterproof Box.

D. Navigation Design

Our proportional control worked using a GPS and magnetometer. Once our GPS fixed six satellites, it took its current position as an origin and navigated to waypoints relative to the origin. The GPS reported the actual location of the robot, and our code calculated the desired yaw for our robot to face its next predetermined waypoint. Then, our onboard magnetometer reported our actual yaw and we calculated our motor control efforts using the difference between our actual and desired yaw multiplied by some gain factor of our choosing. Since our robot had two motors, each offset from the center, we were able to tailor the gain factors of each motor in such a way that our motors had equivalent responses to the same control effort. We were then able to navigate using our calculated motor control efforts.

IV. Modeling

The anemometer and turbidity sensor were modeled using historical data. Wind speed data was obtained from the NASA Modern Era Retrospective Analysis for Research and Applications [20]. Clarity sensors were modeled by using satellite data to mimic the effect seawater has on light intensity. [21]. Turbidity modelling was based off of prior calibrations in lab and observations of Dana Point water during deployment [22].

A. Anemometer

Given that the three cup anemometer design we selected shows a highly linear relationship between rotation rate and wind velocity, a first order model was assumed with rotation rate and miles per hour determined by the equation:

$$V = CR$$

Where $V$is the wind speed, C is the circumference of the anemometer, and R is the rotation rate.

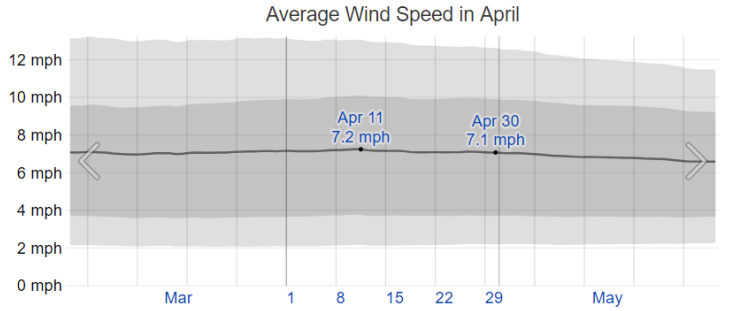

Figure 10: Average Wind Speed in April at Dana Point [20, 23]

Given that the mean wind speed at Dana Point averaged approximately seven miles per hour [20] with gusts of 12 mph, the model above was used to ascertain whether the stated sampling rate was insufficient for the anemometer. Using a higher than average wind speed of 8 mph with a gust of 16 mph (Figure 11), we found that the anemometer had a rapid response time, and did not rotate at a rate that exceeded the sampling rate of the Teensy. The limitations on the model were that it did not take into account the friction at the ball bearing, or the drag on the cups, but since the anemometer was modelled with a view to maximizing the rotation rate based on historical values in order to test sampling efficacy, the model was sufficient.

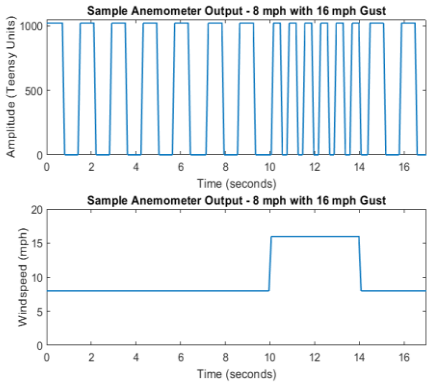

Figure 11: Results of a modeled 8 mph wind with a 16 mph gust

B. Turbidity

Historical turbidity data for Dana Point was unavailable. Given the lack of historical data, underwater footage collected in a previous year at Dana point harbour was used to give an estimate of turbidity values [23]. Based on comparisons with turbidity standards, the turbidity was roughly estimated to be between 300 to 500 NTUs. Below is a modeled turbidity readout for regions of different turbidites with white noise added to replicate field conditions:

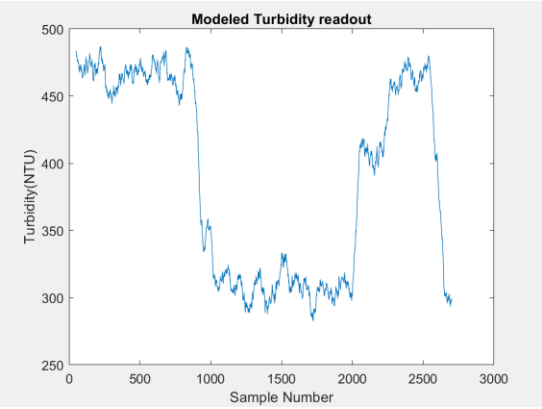

Figure 12: Results of modeled turbidity.

C. Clarity

Light intensity in a medium falls off exponentially as a function of distance, according to the Lambert-Beer Law which states:

$$I_Z = I_0 e^{-xz}$$

Where $I_Z$is the intensity at depth z, I_0 is the surface intensity, and x is the attenuation coefficient for a particular wavelength of light. Given that the submerged clarity sensor is at a depth of 20 cm throughout the entirety of the experiment, z is kept constant. Surface intensity is also assumed constant, given that it undergoes a less than 1% change over the length of a deployment [21]. The attenuation coefficient was estimated to be 0.7, based on satellite data around the Los Angeles coastline [24]. Given that the ratio of photodiode readings is equal to the ratio of light intensities is of primary interest in finding attenuation coefficients, I_Z *and* I_0, the expected reading is then considered to be

$$I_0/I_z = e^{0.7*0.2}$$

Which gives the ratio of the two intensities, and thus the baseline photodiode ratio, as 1.15. We expected some deviation from this ratio due to the considerable human activity on the beach stirring up sand in the shallow water. The combination of a breakwater reducing water circulation and human activity would result in a higher attenuation coefficient value compared to the open ocean. We added some spikes in the ratio to represent these patches of low visibility along with noise to replicate field conditions. Below is a modeled clarity readout for sensors moving in regions of different attenuation coefficients:

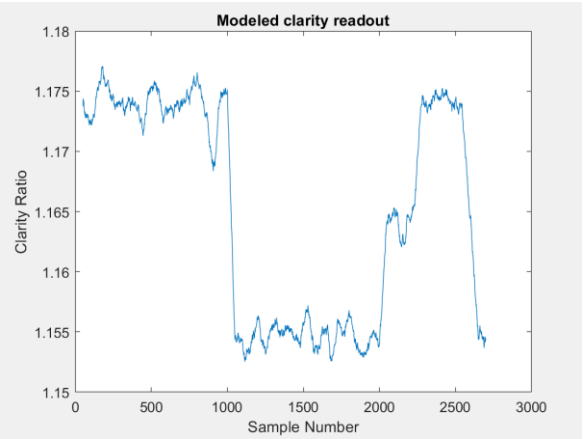

Figure 13: Results of modeled clarity.

V. Experimental Procedure

We deployed our AUV multiple times: once at the Bernard Field Station (BFS), three times at pools across campus, and once at Dana Point. The goal of our first deployment at BFS was to see if we could obtain preliminary data from our different sensors and to see if our robot would be able to autonomously navigate correctly. To begin testing at BFS we first made sure that the Hall sensor was properly connected to the anemometer and that there was nothing blocking the turbidity or the clarity sensors. Then we rowed out to the middle of Phake lake where we started our Teensy code, waited for the GPS to connect to six satellites, and placed our robot in the water to collect data. We had to wait for satellites because our proportional control code did not start navigation without fixing six satellites. From this deployment we found that all of our sensors worked but that our robot did not properly autonomously navigate. As a result, we needed to use the boat to retrieve the robot. Once we retrieved the robot we were able

to download the data files from the SD card and analyze the files using a Matlab script that we wrote.

Since the only thing that did not work at the BFS was navigation, we took the robot to the pool three times to try to fix the navigation. The first pool deployment was focused on creating waypoints and determining how the waypoint directions related to the robot's orientation. However, before we could do this we found that the GPS was not fixing on the appropriate origin thus making it impossible for the AUV to reach the proper waypoints. Originally, we hardcoded the origin as a waypoint. However, due to the inconsistency in the coordinate the GPS reported when it fixed on to six satellites we found that the origin could be a few meters away from the true location of the AUV. This lead to many problems with the navigation between waypoints, since it sometimes caused a waypoint to be outside of the pool. To fix this issue, we changed the code so that the origin was the coordinate the GPS reported when it successfully fixed onto six satellites and every waypoint was thus set relative the this initial GPS coordinate. Despite correcting the problem with the origin and waypoints, we were still having many problems with the reported heading and getting our robot to move in a straight path.

The next time we went to the pool we focused on changing the gains of the motors so that the robot navigated in a straight line when instructed to. While we were able to determine the proper gain values for each motor we still had a major issue with our heading values not being consistent as the robot turned. We later realized that the confusing heading measurements were due to an uncalibrated magnetometer.

After calibrating the magnetometer we took our robot back to the pool to see if that fixed the navigation issues. Unfortunately, there was still a problem with the heading changing sporadically. We determined that this problem was due to the motors being too close to the motherboard box, and moved the motors so they were farther from the motherboard. This fix stabilized heading readings, so we were more confident in our navigation leading up to Dana point deployment.

Once we arrived at Dana Point, we deployed and saw that our AUV still was not navigating as well as we hoped. After some land testing, we found that yaw was not offset properly so that 0 degrees pointed due East, and after a few adjustments to the offset angle, our navigation finally worked. At Dana Point, we would connect the computer to our motherboard, upload the code, and put the AUV into the water before it acquired all six of the required GPS signals. Once it acquired six satellites, it would navigate through the waypoints and return to us at the origin. After almost each deployment, we would upload the data logged on our robot to start data processing.

VI. Data and Results

Over the course of the deployment window, a dozen data logs were recorded. For the sake of this paper we will use one data set as an example. For this run, our turbidity sensor gave us the following readouts for the passthrough photodiode and 90 degree photodiode detection.

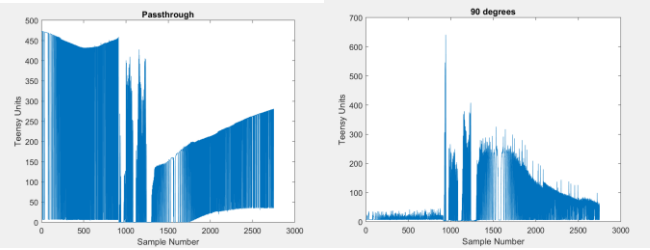

Figure 14: Graphs of passthrough and 90 degree turbidity data.

To analyze our photodiode data, we took the ratio of our 90 degree reading over our passthrough reading in our Matlab script. This served as our turbidity measurement, as more turbid solutions will scatter more light and let less light pass through, and vice versa. Our turbidity data is shown below:

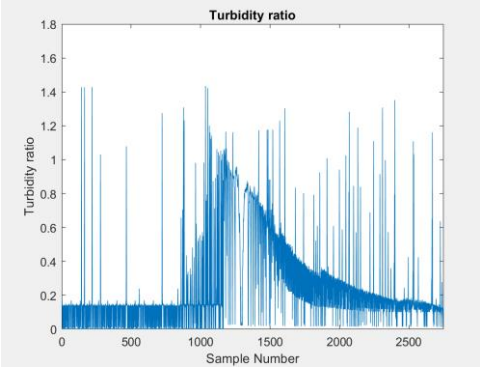

Figure 15: Graph of the ratio of the passthrough to 90 degree turbidity.

We noticed that our turbidity ratio had a lot of high frequency noise associated with it. This was likely due to power supply noise caused by our motors. To eliminate this noise, we passed our signal through a low pass filter:

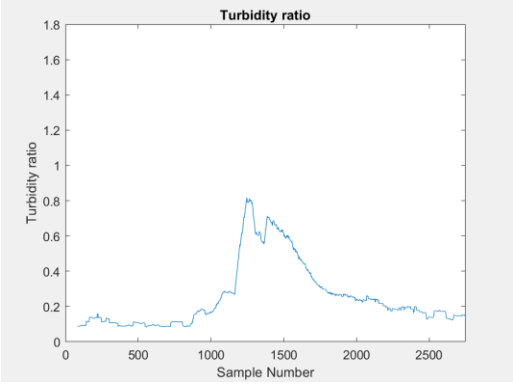

Figure 16: Turbidity data after using a low pass filter.

Importantly, this ratio still does not have any meaningful unit associated with it. To put this in terms of a unit, we created a calibration curve using solutions of known

turbidites with our nephelometer. Our calibration curve is shown below:

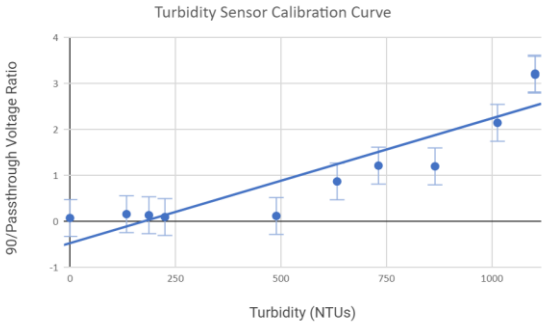

Turbidity(NTU) = (Turbidity Ratio + .465)/.0027

Figure 17:. Turbidity sensor calibration curve and equation

Putting our signal in terms of NTU:

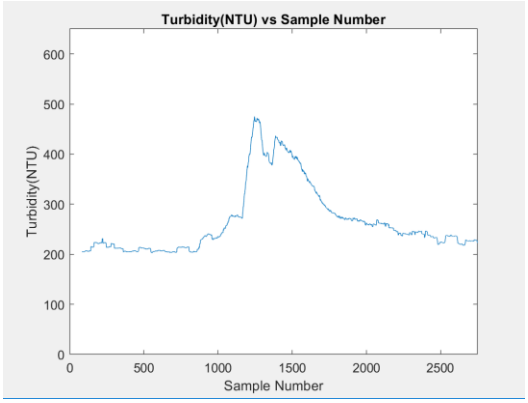

Figure 18: Turbidity data in terms of NTU

Looking at our data, we have a lot of noise, but we seem to have a readout that suggests that we had clear water initially, the robot moved into a more turbid region, and then the robot moved back into clear water.

This finding is supported by our clarity data. For our clarity, we had two arrays of data, one for each photodiode. To get a value that represents clarity, we took the ratio of light detected at the surface over the light detected by the submerged photodiode. This value is representative of clarity because it gives us an idea of the extent that light penetrates the water. Our readout is shown below:

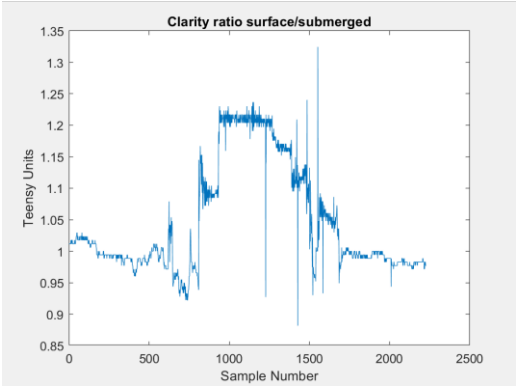

Figure 19: Initial clarity data

This readout has similar high frequency noise to our initial turbidity readout. Passing our readout through a low pass filter, we get:

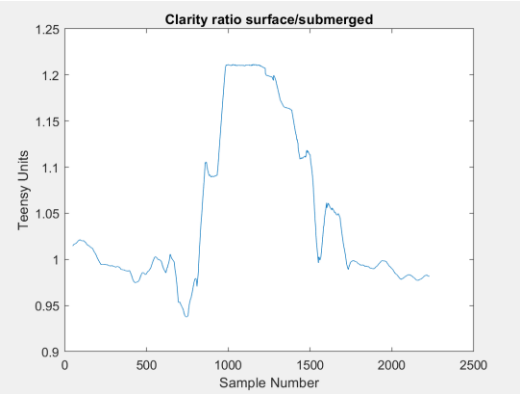

Figure 20: Low pass filtered clarity data

Similarly to our turbidity measurement, we have a region in the middle of our readout where the water is less clear since the surface light measurement is definitively greater than the submerged light measurement. This is more clearly shown below:

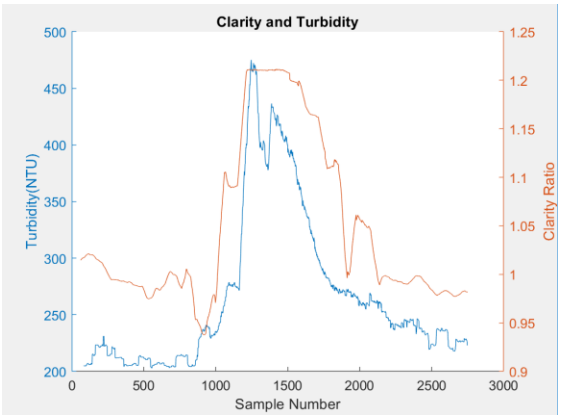

Figure 21: Overlaid clarity and turbidity readouts

From this data, we saw that an 82% increase in turbidity corresponded to a 22% increase in clarity.

Next, we have the data reported by our anemometer. For the same run, we had the following anemometer data.

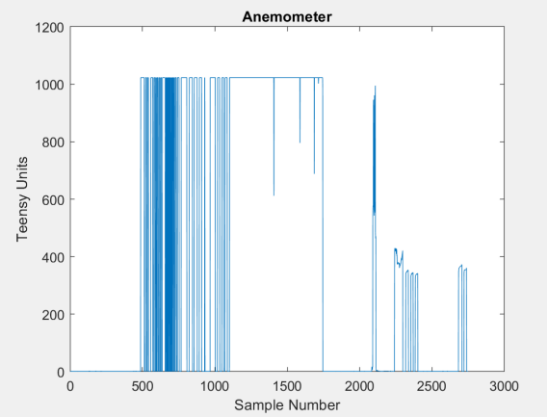

Figure 22: Initial Anemometer data

Here, a nonzero value represents a high measurement on our Hall sensor. So a revolution of our anemometer is represented by a change from low to high. To get meaningful wind speed data, we made a Matlab script that found instantaneous rotation speed from the time since the last revolution along with an average revolution speed. We then translated our revolution speed to wind speed using our anemometer calibration plots [Figures 23, 24].

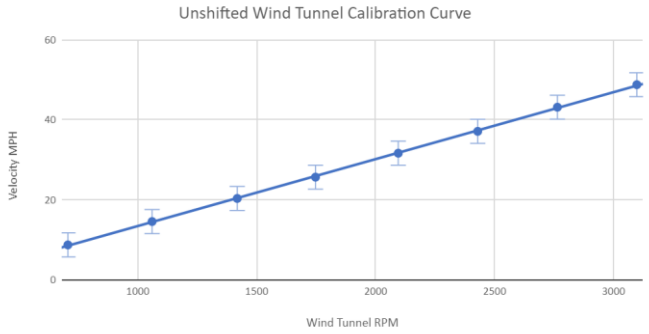

Figure 23: Wind Tunnel Velocity/RPM calibration curve

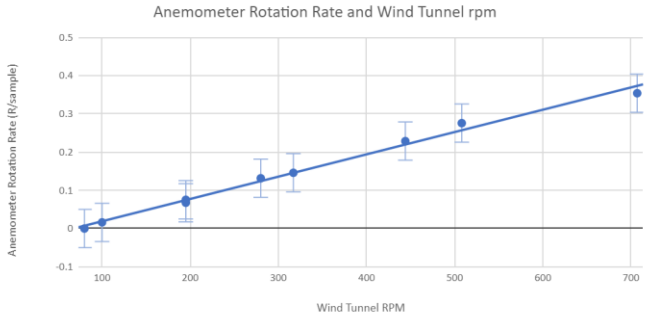

Figure 24: Anemometer Rotation rate/Wind Tunnel RPM calibration curve

Combining the two calibration plots gives the following equation:

MPH = 28.39334*(Average Rotation Rate) - 0.1752331

Converting our anemometer data to wind speeds, we get the following:

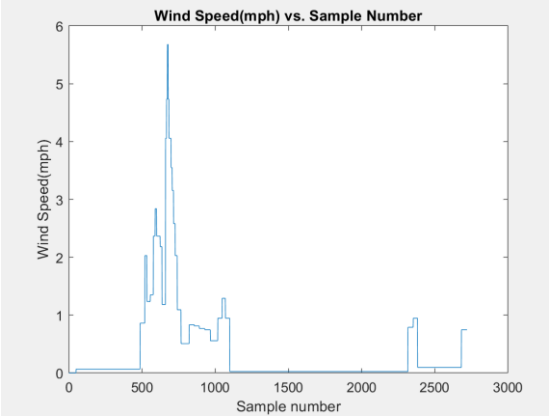

Figure 25: Logged Wind Speed vs Sample Number

Average wind speed = 0.37 ± 0.1 mph

This result does not line up with our turbidity and clarity data. We think that this is the case because the low wind speeds in the harbor do less to increase water turbidity than human activity, so their effect is relatively unpronounced.

Finally, for the same run, we have our GPS readout:

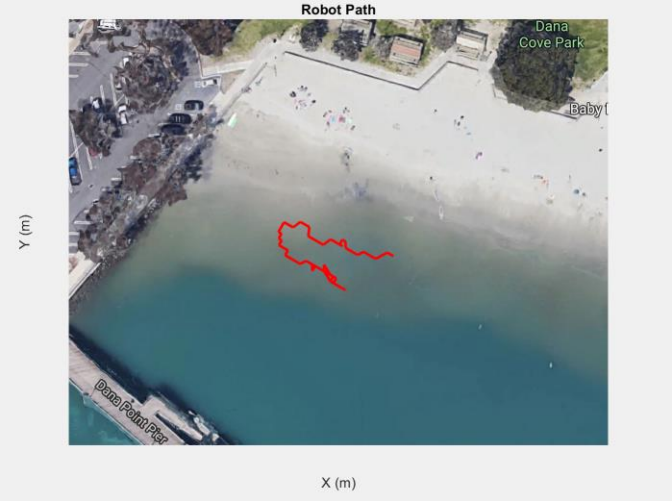

Figure 26: GPS Logged Path at Dana Point

Here, we can see that the robot started near the beach, moved towards the parking lot, and then out towards deeper water.

VII. Comparison of Data to Model

Here, a sensor by sensor approach will be used, comparing usable data to models and then examining ways where our sensor measurements failed.

A. Turbidity

Turbidity data from the successful launch fell well within the predicted outcome, going from relatively clear water at 200 ±20 NTUs to water at a peak turbidity of 590 ±20 NTUs.

B. Anemometer

The measured average windspeed was 0.37± 0.1 mph, contrary to the historical data's prediction of 7.2mph. This could partially be attributed to the presence of the breakwater, and the general sheltered area around which the deployment took place, but the major reason why this reading is a 700% decrease from the expected result is that it is a reading from only one deployment over a brief period of time. Very little wind blew during that deployment, and all anemometer data from later deployments proved unusable due to the hall sensor on the anemometer shorting due to inadequate waterproofing (Figure 27). In order to rectify this and obtain data more in line with the expected values, or perhaps even to prove the wind breaking nature of the breakwater, more data must be collected over a greater period of time.

Figure 27: Anemometer's Hall sensor. Note the incomplete waterproofing, with salt deposits (green)

C. Clarity

Clarity data was within 4% of the modeled value. A calculated value of 1.15 was obtained, and the clarity ratio obtained had a peak of 1.2. This is slightly surprising, as seawater scatters different wavelengths of light to varying degrees, which our model did not take into account, using 490 nm satellite data rather than the full spectral sensitivity range of our photodiodes (400nm-700nm).

VIII. Conclusion

The goals of this project were to create a fully functional AUV capable of navigating between waypoints and collecting data on wind speed, turbidity, and clarity. While we were unable to determine a correlation between wind speed and turbidity from our collected data, we did observe a strong similarity between turbidity and clarity. This similarity makes sense because as the amount of sediment present in the water increases the amount of light that passes through the water, and the amount of light that a person should be able to see should decrease. Although we did not observe a correlation between wind speed and turbidity at the water's surface, this does not mean that there is never a correlation between the two measurements. Since we took data in such shallow water with so many people around, we believe that any observable correlation between wind speed and turbidity was obscured by the increase in turbidity caused by people agitating the sediment from the ocean floor as they were walking and swimming.

In the future, data should be take over a much larger period of time to observe seasonal and even yearly trends. In addition, the robot should be placed in an area of open ocean, away from the shore and not protected by a breakwater. By putting the robot in open ocean, the error in turbidity due to people would be reduced, and there would be fewer barriers present that could block the wind. If given the time, we would also like to take turbidity and clarity measurements just above the ocean floor to see how wind speed can affect turbidity in two different ways. Unfortunately, our Hall effect sensor corroded when it came in contact with the salt from the ocean water due to poor waterproofing, so in the future we would suggest adding clear nail polish to the base of the sensor to improve the waterproofing, as we did with both clarity sensors. Lastly, we suggest reducing the frequency of the LM555 timer in order to prevent aliasing in the future.

IX. Acknowledgements

We would like to thank the entire E80 Teaching team and proctors for answering all of our questions and helping us to make this project a success. We would also like to thank Paul Stovall for helping us to print our turbidity sensor, and for giving suggestions on attaching our anemometer when the specified pieces were not fitting properly. Lastly, we would like to thank the two children on the kayak at Dana Point who stopped rowing when our robot decided to turn abruptly in the water and cut them off.

X. References

[1] E80 Teaching Team, Harvey Mudd College, "E80 Project", https://sites.google.com/g.hmc.edu/e80/project

[2] E80 Teaching Team, Harvey Mudd College, "Reference Anemometer Procedure", https://docs.google.com/document/d/1rY2bEjX3RP1EuHBjaoB50aiPz61I9q4W86KAzeNQdSo/edit

[3] E80 Teaching Team, Harvey Mudd College, "ReferenceAnemometer.zip", https://drive.google.com/file/d/10PVtvyJ87abJO67Chued8QdySKAWsk1L/view

[4] E80 Teaching Team, Harvey Mudd College, "Reference AUV Turbidity Meter Procedure", https://docs.google.com/document/d/1RYaInz-txbC4iaJD83_0HSwKYBlVGDN1HlEs4yDEMjM/edit

[5] E80 Teaching Team, Harvey Mudd College, "ReferenceAUVTurbidityMeter.zip", https://drive.google.com/file/d/10QO_RUk4GNhHB0n_1xPkC-ebEDFHg0sX/view

[6] Diodes Incorporated, “Ultra High Sensitivity Micropower Omnipolar Hall-Effect Switch,” AH9246, datasheet, https://www.diodes.com/assets/Datasheets/AH9246.pdf
[7] API, “Infrared Rejection Filter Planar Photodiode,” SLD-70BG2, datasheet, https://media.digikey.com/pdf/Data%20Sheets/Photonic%20Detetectors%20Inc%20PDFs/SLD-70BG2.pdf
[8] Microchip, “2.7V to 6V Single Supply CMOS Op Amps,” MCP601, datasheet, http://ww1.microchip.com/downloads/en/DeviceDoc/21314g.pdf
[9] Jameco Electronics, “PIN Silicon Photodiode,” OP950, datasheet, https://datasheet.octopart.com/OP950-TT-datasheet-7617992.pdf
[10] Everlight, “Technical Data Sheet 5mm Infrared LED, T-1 ¾,” IR1503, datasheet, https://media.digikey.com/PDF/Data%20Sheets/Everlight%20PDFs/9-IR1503.pdf
[11] Texas Instruments, “LM555 Timer,” LM555, http://www.ti.com/lit/ds/symlink/lm555.pdf
[12] Texas Instruments, “μA78xx Fixed POsitive Voltage Regulators,” μA78xx, datasheet, http://www.ti.com/lit/ds/symlink/ua78.pdf
[13] Adafruit, “Radial Ball Bearing 608ZZ - Set of 4,” https://www.digikey.com/product-detail/en/adafruit-industries-llc/1178/1528-1909-ND/5356858
[14] Radial Magnet Inc., 9049, https://www.digikey.com/product-detail/en/radial-magnet-inc/9049/469-1075-ND/6030786
[15] E80 Default_Robot.ino, Arduino Code
[16] E80 Default Robot Libraries
[17] Staff, F. (2019). *Turbidity*. [online] Environmental Monitor. Available at: https://www.fondriest.com/news/turbidity.htm [Accessed 4 May 2019].
[18] Environmental Measurement Systems. (2019). *Water Temperature - Environmental Measurement Systems*. [online] Available at: https://www.fondriest.com/environmental-measurements/parameters/water-quality/water-temperature/ [Accessed 4 May 2019].
[19] Cho, H. (2019). *Effects of Prevailing Winds on Turbidity of a Shallow Estuary*. [online] PubMed Central (PMC). Available at: https://www.ncbi.nlm.nih.gov/pmc/articles/PMC3728585/ [Accessed 4 May 2019].
[20] NASA Modern-Era Retrospective Analysis for Research and Applications Available at: https://gmao.gsfc.nasa.gov/reanalysis/MERRA-2/
[21] J. Liu, W. Zhang, ‘The Influence of the Environment and Clothing on Human Exposure to Ultraviolet Light’, Public library of science, Available at https://www.researchgate.net/figure/Ultraviolet-light-intensity-at-different-times-in-three-types-of-weather-mW-cm2_fig11_275660564
[22] E80 Teaching Team, Harvey Mudd College https://drive.google.com/file/d/0B0LRqzf8SR2IUlFOUkpiZUxKdjQ/view
[23] Visualization from https://weatherspark.com/m/1838/4/Average-Weather-in-April-in-Dana-Point-California-United-States
[24]Wei Shi, and Menghua Wang,” Characterization of global ocean turbidity from Moderate Resolution Imaging Spectroradiometer ocean color observations’, Journal of Geophysical research https://agupubs.onlinelibrary.wiley.com/doi/pdf/10.1029/2010JC006160